# The photoelectron spectrum of $CCl_2^-$: the convergence of theory and experiment after a decade of debate†

**Scott W. Wren,[a] Kristen M. Vogelhuber,[a] Kent M. Ervin[b] and W. Carl Lineberger*[a]**

***Received 17th December 2008, Accepted 12th February 2009***
***First published as an Advance Article on the web 20th April 2009***
**DOI: 10.1039/b822690c**

We report new 351 nm negative ion photoelectron spectra of $CCl_2^-$, $CBr_2^-$, and $CI_2^-$. This study was undertaken in an attempt to understand the major discrepancy between dihalocarbene ($CX_2$, X = Cl, Br, I) singlet–triplet splittings reported by our laboratory (R. L. Schwartz, G. E. Davico, T. M. Ramond, W. C. Lineberger, J. Phys. Chem. A., 1999, **103**, 8213) and new theoretical values. Our recent experiments show that a dihalomethyl anion ($CHX_2^-$) contaminant in the dihalocarbene anion beam, previously considered insignificant, made a major contribution to the reported $CX_2^-$ photoelectron spectra. Thus, the interpretations of the earlier $CX_2^-$ spectra and the reported singlet–triplet splittings were incorrect. Replacing $O^-$ with $OH^-$ in the anion formation process yields a pure dihalomethyl anion, whose highly structured photoelectron spectrum can be subtracted from the contaminated spectrum, yielding a clean $CX_2^-$ photoelectron spectrum. The new $CCl_2^-$ photoelectron spectrum displays resolved vibronic transitions to the two lowest electronic states of $CCl_2$: $X^1A_1$ and $a^3B_1$. The electron affinity of $X^1A_1$ $CCl_2$ is 1.593(6) eV. A large change in geometry between the anion and the neutral triplet state precludes the direct observation of the triplet origin. The energy difference between the $X^1A_1$ and $a^3B_1$ states of $CCl_2$ is estimated to be $\sim$0.9(2) eV, consistent with high-level theoretical studies. While we confirm similar dihalomethyl anion contaminants in the earlier photoelectron spectra of $CBr_2^-$ and $CI_2^-$ and report new photoelectron spectra for these ions, the paucity of resolved features in the spectra provides limited additional thermochemical information.

## Introduction

Carbenes (:CXY) are highly reactive diradicals with two electrons occupying nearly degenerate σ and π orbitals. They serve as intermediates in many chemical reactions, including addition to a double bond, insertion into a single bond, dimerization, and intramolecular rearrangement.[1–4] The nature of the substituents affects whether the electronic configuration of the ground state is a $\sigma^2$ singlet or a diradical $\sigma^1\pi^1$ triplet.[4] The singlet $^1A_1$ and triplet $^3B_1$ states lie close in energy but exhibit very different reactivities, so the difference in energy between the two states ($\Delta E_{ST}$) is a quantity of great interest. Furthermore, dihalocarbenes have served as test cases for comparing experimental and theoretical energy splittings. For these reasons, carbenes have drawn attention from both experimental and theoretical research groups for decades.

Singlet–triplet energy splittings are difficult to determine experimentally.[4] Though the singlet ground states of the dihalocarbenes have been well-characterized,[5–18] spectroscopic methods are commonly unable to interrogate states of different multiplicity, making $\Delta E_{ST}$ an elusive quantity. Extensive theoretical work has been done to calculate $\Delta E_{ST}$ of the dihalocarbenes. In the late 1980s, Carter and Goddard[19–21] carried out one of the first thorough studies to determine the magnitude of $\Delta E_{ST}$ of neutral dihalocarbenes. More calculations followed,[22–25] and the computational results reached a consensus that the $^3B_1$ states of $CCl_2$, $CBr_2$, and $CI_2$ lie 10–35 kcal mol$^{-1}$ higher in energy than their respective $^1A_1$ states.

Anion photoelectron spectroscopy is a direct method of measuring $\Delta E_{ST}$. In 1999, Lineberger and co-workers investigated the series of dihalocarbenes $CX_2$ (X = F, Cl, Br, I) with this technique.[26] The singlet–triplet splitting obtained from the spectrum of $CF_2^-$ ($\Delta E_{ST}$ = 54(3) kcal mol$^{-1}$)[26] agreed with theoretical predictions ($\Delta E_{ST}$ = 56.9(7) kcal mol$^{-1}$),[27] but the splittings for the heavier dihalocarbenes did not.[27] Theorists calculated a $\Delta E_{ST}$ of $\sim$20 kcal mol$^{-1}$ for $CCl_2$ and $\sim$17 kcal mol$^{-1}$ for $CBr_2$,[22–25] while the photoelectron spectra implied substantially lower $\Delta E_{ST}$ values: 3(3) kcal mol$^{-1}$ for $CCl_2$, and 2(3) kcal mol$^{-1}$ for $CBr_2$. Recently, more calculations have followed as rapid advances in theory have been made.[27–35] Of particular interest was $CCl_2$, the most computationally tractable of the dihalocarbenes. Notably, Dyke and co-workers performed a combined *ab initio*, Franck–Condon study to simulate the $CCl_2^-$ photoelectron spectrum.[33] All calculations yielded the larger $\Delta E_{ST}$ values, consistent with the earlier

[a] *JILA and Department of Chemistry and Biochemistry, University of Colorado, 440 UCB, Boulder, CO, 80309, USA. E-mail: wcl@jila.colorado.edu*
[b] *JILA Visiting Fellow, Department of Chemistry and Chemical Physics Program, University of Nevada, 2008, Reno, NV, 89557-0216, USA*

† Electronic supplementary information (ESI) available: Geometries, frequencies, and normal mode vectors used in simulations as well as expanded and enhanced figures. See DOI: 10.1039/b822690c

theoretical studies. This discrepancy between theory and experiment prompted us to carry out a careful reinvestigation of the photoelectron spectra of the dihalocarbenes, particularly $CCl_2^-$.

We have carefully examined the chemistry taking place in the ion source, and we have identified contamination from $CHCl_2^-$ in the previously reported $CCl_2^-$ spectrum that had obscured the triplet band and skewed $\Delta E_{ST}$. In the current study, we collect the photoelectron spectrum of pure $CHCl_2^-$ and minimize its contribution to elucidate the $CCl_2^-$ experimental data. We present the $CCl_2^-$ 351 nm photoelectron spectrum that exhibits vibrationally resolved transitions to singlet and triplet electronic states, yielding substantially improved agreement with high-level calculations. We then show that the halomethyl anions $CHBr_2^-$ and $CHI_2^-$ also had contaminated the previous photoelectron spectra of $CBr_2^-$ and $CI_2^-$.[26] A detailed study of the halomethyl anions is underway and will be reported in a future publication.[36]

## Experimental methods

The negative ion photoelectron spectrometer used in this experiment has been described in detail elsewhere.[37–39] The apparatus consists of three main sections: an ion source, a mass filter, and an interaction region. Negative ions are formed in a flowing afterglow ion source. A microwave discharge containing trace amounts of $O_2$ gas in He buffer gas ($\sim$0.4 Torr) generates atomic oxygen radical anion, $O^-$. The appropriate $CH_2X_2$ dihalomethane precursor ($CH_2Cl_2$, $CH_2Br_2$, or $CH_2I_2$, Sigma-Aldrich) is added downstream, where it can undergo a variety of reactions with $O^-$; namely, $H_2^+$ abstraction to produce $CX_2^- + H_2O$, $H^+$ abstraction to produce $CHX_2^- + OH$, O addition to produce $X^- + OCH_2X$, and H abstraction to produce $OH^- + CHX_2$. Collisions with He buffer gas vibrationally cool the ions to approximately 350 K. As described in more detail later, we employ a different reaction sequence using hydroxide ($OH^-$) reactant ion to produce $CHX_2^-$ dihalomethyl anions exclusively. The flow tube can be cooled with a liquid nitrogen jacket to obtain a cold spectrum of ions with vibrational temperatures near 200 K. Anions are extracted into a differentially pumped region and are accelerated to 735 eV before entering a Wien velocity filter with a mass resolution of $m/\Delta m \approx 40$. The mass-selected ion beam (typically 200–500 pA) is decelerated to 35 eV and focused into the interaction region. Here, the $\sim$0.5 W output from a single-mode continuous-wave argon ion-laser operating at either 351 nm (3.531 eV) or 364 nm (3.408 eV) is built up to approximately 100 W of circulating power in an optical buildup cavity located within the vacuum system. The laser beam intersects the ion beam perpendicularly, ejecting electrons from the anions. Electrons ejected into a small solid angle orthogonal to both the laser and ion beams enter a hemispherical energy analyzer and are then imaged onto a position-sensitive detector. The number of ejected electrons is recorded as a function of kinetic energy. The energy analyzer has a resolution of approximately 10 meV.

The electron kinetic energy (eKE) can be converted to electron binding energy (eBE) through the relationship eBE = $h\nu$ − eKE. Absolute kinetic energies are calibrated[40] before each experiment using the well-known electron affinity of O.[41] Additionally, the energy scale is corrected for a slight linear compression ($<1\%$)[37] using the photoelectron spectrum of $W^-$, which provides a number of known transitions spanning the photoelectron energy range.[42] After making these corrections and accounting for the resolution of the spectrometer and rotational peak profiles, absolute electron binding energies can be determined with an accuracy of 5 meV or better.[37]

A rotatable half-wave plate positioned outside the buildup cavity controls the polarization of the photodetachment radiation. When the angle between the laser polarization and the direction of the collected electrons is 54.7°, referred to as the magic angle, the photoelectron spectrum is independent of the anisotropy parameter of the ejected electrons.[43] Therefore, spectra collected at the magic angle directly reflect the total photodetachment cross-section. All spectra shown here were collected with magic-angle polarization unless otherwise noted.

## Theoretical methods

Electronic structure calculations were carried out using the Gaussian 03 software package.[44] All calculations for $CCl_2$ use the coupled-cluster CCSD(T) method[45] with an augmented correlation-consistent polarized triplet-zeta basis set (aug-cc-pVTZ).[46,47] Calculations for $CBr_2$ were performed with density functional theory at the B3LYP/6-311++G(d,p) level.[48,49] Geometries were optimized and harmonic vibrational frequencies and normal mode coordinates were calculated for the doublet anion and the singlet and triplet neutral states. Calculated harmonic frequencies are reported without applying a scaling factor. Salient results of the calculations are given in Tables 1–3, with additional details available in the ESI†.

**Table 1** Energies of origin transitions, vertical detachment energies, and singlet–triplet splittings ($\Delta E_{ST}$) of dihalocarbenes (eV)

| | | $X^1A_1 \leftarrow X^2B_1$ | | $a^3B_1 \leftarrow X^2B_1$ | | |
|---|---|---|---|---|---|---|
| | | (0–0) | VDE | (0–0) | VDE | $\Delta E_{ST}$ |
| $CCl_2$ | This work | 1.593(6) | 2.00 | 2.47(20) | >3.2 | 0.9(2) |
| | Theoretical[a] | 1.586 | 1.910 | 2.481 | 3.401 | 0.895 |
| $CBr_2$ | This work | 1.78(10) | 2.25 | >1.9 | — | — |
| | Theoretical[b] | 1.834 | 2.400 | 2.579 | 3.719 | 0.745 |
| $CI_2$ | This work | <3 | — | — | — | — |
| | Theoretical[b] | 2.095 | 2.537 | 2.500 | 3.535 | 0.39 |

[a] CCSD(T)/aug-cc-pVTZ (this work). [b] Single-point RCCSD(T)/ECP28MWB- and ECP46MDF-basis sets[29]

 

**Table 2** Spectroscopic quantities and molecular constants of $CCl_2$

| | | $r$/Å | $\theta$/° | $\nu_1$/cm$^{-1}$ | $\nu_2$/cm$^{-1}$ | $\nu_3$/cm$^{-1}$ |
|---|---|---|---|---|---|---|
| $CCl_2^-$ $X^2B_1$ | This work | 1.90(2)[a] | 104(2)[a] | 500(100) | 200(100) | — |
| | Experimental[b] | 1.92(2) | 103(2) | — | — | — |
| | Theoretical[c] | 1.892 | 103.75 | 547.6 | 243.3 | 463.3 |
| $CCl_2$ $X^1A_1$ | This work | — | — | 737(6) | 339(10) | — |
| | Experimental | 1.714(1)[d] | 109.3(1)[d] | 731.14(22)[e] | 335.79(11)[e] | 745[f] |
| | Theoretical[c] | 1.729 | 109.02 | 728.7 | 333.7 | 758.1 |
| $CCl_2$ $a^3B_1$ | This work | 1.69(10)[a] | 127(10)[a] | ~600[g] | 300(20)[g] | — |
| | Theoretical[c] | 1.684 | 127.40 | 681.6 | 296.8 | 992.6 |

[a] Geometry changes are computed using Franck–Condon analysis. Absolute geometries are determined using as reference the experimental LIF geometrical parameters[18] of $X^1A_1$ $CCl_2$. [b] Photoelectron spectroscopy.[57] [c] CCSD(T)/aug-cc-pVTZ (this work). [d] LIF.[18] [e] Dispersed fluorescence.[51] [f] Excitation matrix.[14] [g] Value obtained from peak separations at high vibrational quantum numbers (10–12) and simulations of extent of progressions based on calculated geometries. See text.

**Table 3** Spectroscopic quantities and molecular constants of $CBr_2$

| | | $r$/Å | $\theta$/° | $\nu_1$/cm$^{-1}$ | $\nu_2$/cm$^{-1}$ | $\nu_3$/cm$^{-1}$ |
|---|---|---|---|---|---|---|
| $CBr_2^-$ $X^2B_1$ | This work | 2.09(2)[b] | 105(4)[b] | — | — | — |
| | Theoretical[a] | 2.100 | 106.36 | 455.8 | 129.7 | 365.8 |
| $CBr_2$ $X^1A_1$ | This work | — | — | 600(50) | 200(50) | — |
| | Experimental | 1.865[c] | 110.7[c] | 606.6(4)[d] | 199.5[d] | 679.8(7)[d] |
| | Theoretical[e] | 1.898 | 110.0 | 601.6 | 196.6 | 655.3 |
| $CBr_2$ $a^3B_1$ | This work | — | — | — | — | — |
| | Theoretical[e] | 1.839 | 129.5 | 533.6 | 185.4 | 878.7 |

[a] B3LYP/6-311++G** (this work). [b] Geometry changes are computed using Franck–Condon analysis. Absolute geometries are determined using as reference the experimental LIF geometrical parameters[17] of $CBr_2$ $X^1A_1$. [c] Combined LIF[17] and theory.[61] [d] Single vibronic level emission.[52] [e] CCSD(T)/cc-pVTZ.[29]

The Franck–Condon profiles of the photoelectron spectra are simulated using the PESCAL program, which was modified for this work to simulate transitions among multiple electronic states simultaneously.[50] The simulations start with the theoretical geometries, normal mode vectors, and vibrational frequencies of the anion and neutral states. For the $X^1A_1$ $CCl_2$ and $X^1A_1$ $CBr_2$ singlet states, however, the harmonic frequencies, anharmonicities, and geometries from high-resolution spectroscopy experiments[14,17,18,51,52] (Tables 2 and 3) are used in the simulations instead of the calculated values. For the singlet state transitions, the anharmonicities are significant and known experimentally, whereas the calculated Duschinsky rotation angles between normal mode vectors of the two active modes are modest (5.3° for $CCl_2$ and 9.6° for $CBr_2$). Therefore, the Franck–Condon factors for the singlet state are calculated in the Morse oscillator, parallel mode approximation using numerically integrated Laguerre polynomial wavefunctions.[53] For the $CCl_2$ triplet state transition, the anharmonicities are unknown experimentally, and the calculated Duschinsky rotation angle is significant (17.5°), so the Franck–Condon factors are calculated in the harmonic oscillator approximation but including Duschinsky rotation using the Sharp–Rosenstock–Chen method.[54,55]

The individual vibronic peak contours are obtained by calculating the rotational spectrum, treating the molecules approximately as prolate tops, and convoluting the rotational transitions with the instrumental resolution function, approximated as a Gaussian function with a FWHM of 12 meV. This procedure directly accounts for the small (typically <4 meV) displacement of the rotationless origin of a peak from the location of its maximum intensity. Finally, the normal mode displacements between the anion and the neutral for the Franck–Condon active modes (symmetric stretch and bend), along with the positions of the origin transitions, are adjusted from the theoretical values to match the experimental spectra.

The Wien filter partially resolves the $^{12}C^{35,37}Cl_2^-$ and $^{12}C^{79,81}Br_2^-$ ions; calculated frequencies and rotational constants indicate that the presence of more than one isotope will produce negligible broadening. Thus, isotope issues are neglected in the analysis.

## Results and discussion

In the previous dihalocarbene studies and in the work presented in this paper, the dihalocarbene target anions are produced by reacting $O^-$ with $CH_2X_2$ (X = Cl, Br, I).[56] As a specific example, reactions involving $CH_2Cl_2$ are described in detail below. A variety of reactions occur when $O^-$ reacts with $CH_2Cl_2$ at 300 K, leading to the formation of products with the following branching fractions:[56]

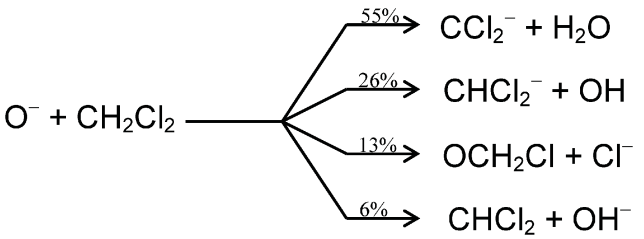

Abstraction of $H_2^+$ by $O^-$ occurs with 55% yield to produce the desired $CCl_2^-$; however, $CHCl_2^-$ produced by proton abstraction, with $m/z$ only 1 amu greater than the desired product, is a significant minor ionic reaction product. Since the Wien filter has a mass resolution of at best $m/\Delta m \approx 40$, we can only partially separate ions within 1 amu of each other at $m/z \approx 80$, specifically $CCl_2^-$ and $CHCl_2^-$. It was initially anticipated that the electron affinity of $CHCl_2$ was sufficiently low that it would not be an important contaminant in the $CCl_2^-$ photoelectron spectrum. However, the significant difference between the experimental[26] and calculated[33] photoelectron spectra of $CCl_2^-$, as well as of the heavier dihalocarbenes,[29] has led us to investigate the dihalomethyl anionic product of this reaction as a possible cause of the discrepancy.

In order to evaluate the $CHCl_2^-$ contribution to the $CCl_2^-$ spectrum, we replace $O^-$ with $OH^-$ in the above reaction. Only the dihalomethyl anionic product is now formed,

$$OH^- + CH_2Cl_2 \rightarrow CHCl_2^- + H_2O$$

Hydroxide ion is formed by reacting $O^-$ with methane in the flow tube. Sufficient methane is added to ensure complete removal of $O^-$ before $CH_2Cl_2$ is introduced and guarantee that $CHCl_2^-$ is the only species present near $m/z \approx 83$.

The photoelectron spectrum of $CHCl_2^-$ is remarkably broad and exhibits extensive vibrational structure. Comparison to the earlier data shows conclusively that dihalomethyl anion contamination was present in the previously reported photoelectron spectrum of $CCl_2^-$ and is responsible for the bulk of the progression previously attributed[26] to the triplet state of $CCl_2$. Spectra of $CHBr_2^-$ and $CHI_2^-$, similarly broad and highly structured, overlap with the spectra of the corresponding dihalocarbene anion, indicating that dihalomethyl anion contamination was also present in the photoelectron spectra of $CBr_2^-$ and $CI_2^-$.[26]

We take several steps to obtain dihalocarbene anion photoelectron spectra with minimal contamination. We first minimize $CHX_2^-$ contribution to the contaminated spectrum by tuning the Wien mass filter to 50% of the maximum on the low-mass side of the appropriate unresolved mass peak. In the synthesis of $CCl_2^-$, we took the additional step of using deuterated dichloromethane precursor ($CD_2Cl_2$) to increase the mass difference between $CCl_2^-$ and $CDCl_2^-$, improving our ability to separate the two ions with the Wien filter. As this approach is less effective for the heavier dihalocarbenes, $CH_2Br_2$ and $CH_2I_2$ precursors were used to make $CBr_2^-$ and $CI_2^-$, respectively. Next, the appropriately scaled authentic $CHX_2^-$ photoelectron spectrum is subtracted from the two-component spectrum. The multiple peaks that are attributable solely to dihalomethyl anion are used to determine the scaling factor. The final constraint is that the scaling factor must leave the subtracted spectrum everywhere as non-negative. As discussed below, this procedure was applied to each of the dihalocarbenes, but the amount of new information gained diminished for the heavier dihalocarbenes.

## $CCl_2$

We obtain a 351 nm photoelectron spectrum of $CCl_2^-$ that clearly resolves both the $X^1A_1$ and $a^3B_1$ electronic states of the carbene. By tuning the Wien filter to the low-mass side of the mass peak containing both $CCl_2^-$ and $CDCl_2^-$, the dihalomethyl anion contribution to the photoelectron spectrum is considerably reduced from that previously reported.[26] Fig. 1a shows the previous 364 nm photoelectron spectrum reported by Schwartz *et al.*[26] Fig. 1b depicts the new 351 nm spectrum that contains a signal from both $CCl_2^-$ and $CDCl_2^-$ (black trace). The 351 nm pure $CDCl_2^-$ photoelectron spectrum obtained under the same experimental conditions is shown in red in Fig. 1b, highlighting the contamination in the $CCl_2^-$ spectrum. There is very good overlap between the pure $CDCl_2^-$ spectrum and the progression centered at 2.7 eV in the contaminated $CCl_2^-$ spectrum. The contribution due to pure $CDCl_2^-$ is subtracted from the contaminated $CCl_2^-$ spectrum in Fig. 1b to produce the clean $CCl_2^-$ photoelectron spectrum shown in Fig. 2a. Some residual $CDCl_2^-$ contamination is seen as regular structure between 2.5 and 2.7 eV because of the slight difference in the peak widths of the two data sets. A magnified view of these spectra is provided in the ESI† to illustrate the subtraction procedure employed here.

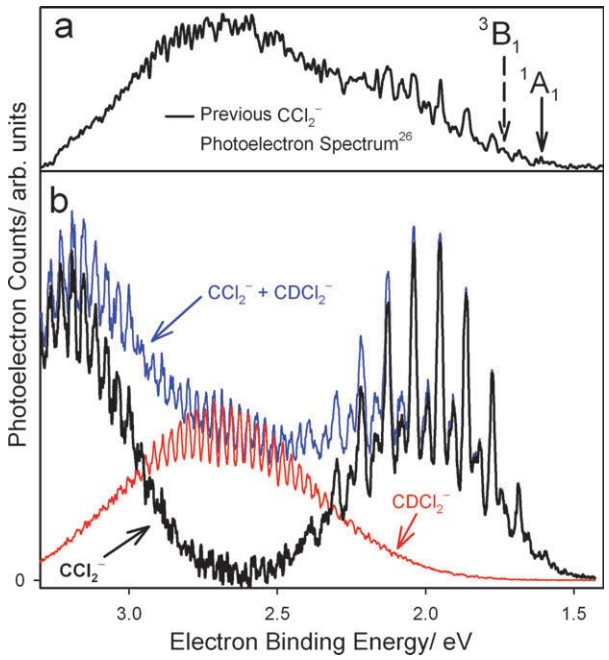


**Fig. 1** $CCl_2^-$ magic-angle photoelectron spectra. (a) The 364 nm $CCl_2^-$ spectrum from the previous study.[26] (b) The new 351 nm spectrum collected at $m/z \approx 81$ minimizes the $CDCl_2^-$ contamination. The pure $CDCl_2^-$ spectrum is scaled and subtracted from the $m/z \approx 81$ trace to yield the "clean" $CCl_2^-$ spectrum.

Fig. 2a shows the clean $CCl_2^-$ photoelectron spectrum from Fig. 1b together with a 364 nm spectrum of $CCl_2^-$ that have both been corrected for $CDCl_2^-$ contamination. The 364 nm cold spectrum of $CCl_2^-$ was obtained while the source flow tube region was cooled with liquid nitrogen. Cooling the flow tube reduces the vibrational temperature of the ions and therefore reduces hot band contributions to the photoelectron spectrum. Fig. 2b shows the simulated spectrum obtained using the PESCAL program. The intensity of the hot band transitions in the singlet state is consistent with a vibrational

 

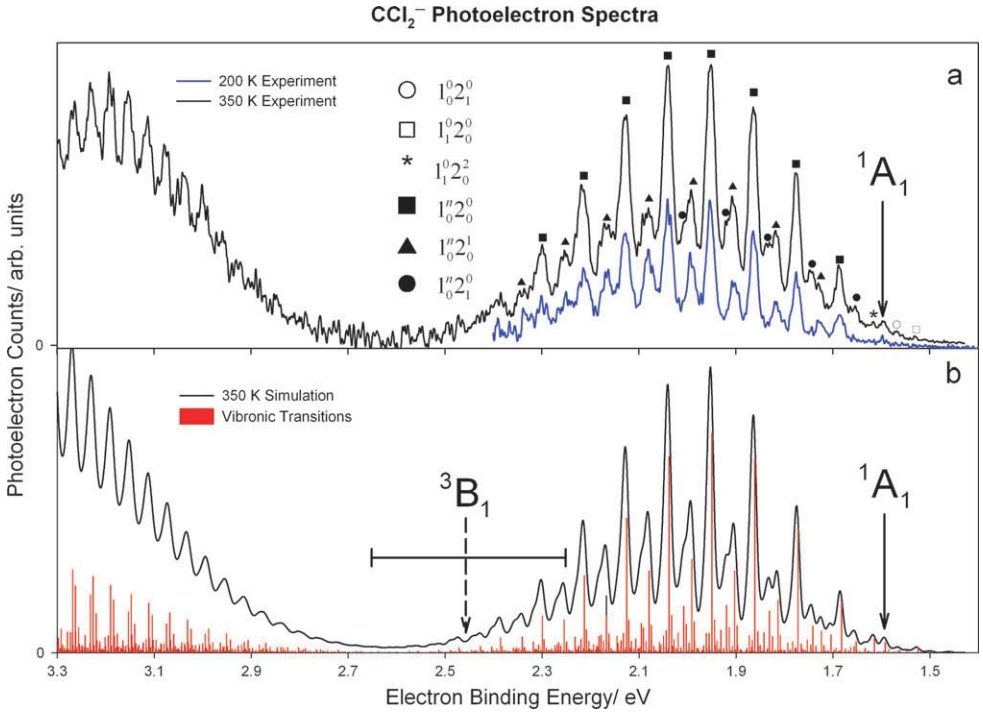


**Fig. 2** Analysis of the photoelectron spectrum of $CCl_2^-$. (a) The experimental magic-angle spectrum was collected at room temperature (upper trace) and at ~200 K (lower trace). (b) Simulated photoelectron spectrum computed at 350 K. The singlet and triplet origins are marked with solid and dashed arrows, respectively. Sticks represent individual vibronic transitions.

temperature of 350 K for $CCl_2^-$. Both the simulated and experimental spectra are limited to an upper binding energy of 3.3 eV because slow electrons (eKE < ~0.3 eV) are not transmitted through the hemispherical energy analyzer. As a result, spectral features from electrons detached near threshold lose intensity. An instrument-related sharp drop-off and the erroneous appearance of a maximum in the Franck–Condon envelope appear at 3.2 eV, which represents a lower limit for the triplet state VDE. The CCSD(T)/aug-cc-pVTZ calculation gives a triplet VDE of 3.401 eV (Table 1), slightly beyond the usable range of our spectrometer.

The photoelectron spectrum of $CCl_2^-$ in Fig. 2a has improved energy resolution over the previous photoelectron experiments,[26] a result of several instrumental improvements and of optimization of the ion-laser intersection position relative to the electron energy analyzer optics. Additionally, we now resolve features at higher electron binding energy because higher photon energy is available with 351 nm excitation and because $CDCl_2^-$ contamination has been subtracted. The origin peak of the singlet $X^1A_1$ state is marked with a solid arrow and is seen in both the room temperature and cold spectra. Our experimental measurement for EA($X^1A_1$ $CCl_2$) of 1.593(6) eV, which includes a rotational peak shift of $-4 \pm 1$ meV, is in good agreement with previous experimental assignments and has improved accuracy.[26,57] The cold spectrum shows a significant reduction in several peak intensities relative to the room temperature spectrum. This observation, along with measured progression peak spacing, enables the assignment of hot bands within the singlet manifold and further confirms the identity of the origin peak.

We observe three distinct vibrational progressions in the singlet state, which are identified in Fig. 2a. The dominant progression arises from the symmetric stretch vibration. A series of doublet peaks lie between the symmetric stretch peaks; the lower eBE peaks arise from combination bands involving the $\nu_1$ symmetric stretch combined with one quantum of the $\nu_2$ bending vibration, denoted $1_0^n2_0^1$. The higher eBE component of each doublet arises from the hot band progression $1_0^n2_0^1$. The two peaks with lower binding energy than the origin are hot bands involving the symmetric stretch and bending vibrations in the $CCl_2^-$ anion. From these progressions, vibrational frequencies of the $X^2B_1$ anion and neutral $X^1A_1$ states are determined and reported in Table 2.

The simulation of the $X^1A_1$ state of $CCl_2$ reproduces all of the resolved peaks in the experimental spectrum. Furthermore, the peak positions and assignments agree quite well with the earlier and more precise dispersed fluorescence measurement of $X^1A_1$ $CCl_2$ vibrational frequencies.[51] The extended progressions also enable an estimate of the anharmonicity of the symmetric stretch vibration, consistent with previous measurements.[51,58] The simulation indicates that several transitions contribute to each peak in the singlet state, although the contributions are minor. For example, the bending vibration ($\nu_2$) is approximately half the frequency of the symmetric stretch vibration ($\nu_1$), which results in the $1_0^n2_0^2$ progression contributing intensity to the symmetric stretch progression. Likewise, the $1_0^n2_0^3$ progression adds a minor contribution to the intensity of the $1_0^n2_0^1$ peaks. The fundamental bending vibration $1_0^02_0^1$ peak cannot be observed in our spectrum because of its low intensity and spectral congestion. These observations are consistent with previous high-level simulations of the $CCl_2$ photoelectron spectrum.[27]

We assign the broad spectral feature at higher binding energy to the $a^3B_1$ excited state of $CCl_2$. The progression has

an apparent onset at ~2.7 eV and has a Franck–Condon vibrational envelope that extends beyond the region accessible with our apparatus. The well-structured progression is very regular with peaks having a FWHM of 30 meV spaced by 300 $cm^{-1}$. The width is a factor of two greater than the instrument resolution, indicating that more than one transition lies beneath each of the triplet peaks. The extended progression also indicates that a large geometry change occurs in both the C–Cl bond length and the Cl–C–Cl bond angle when an electron is ejected from the $X^2B_1$ state of the anion to produce the $a^3B_1$ state of neutral $CCl_2$. Calculations confirm this observation (Table 2), with computed differences in C–Cl bond length and Cl–C–Cl bond angle of the $X^2B_1$ and $a^3B_1$ states of 0.2 Å and 23°, respectively. Such large geometry changes make the interpretation of the photoelectron spectrum more challenging.[59]

The triplet origin cannot be identified in the spectrum for several reasons. First, the large geometry change between $X^2B_1$ $CCl_2^-$ and $a^3B_1$ $CCl_2$ results in a very small Franck–Condon overlap between the ground vibrational levels of the nuclear wavefunctions of the anion and the $a^3B_1$ state of the neutral. The calculated CCSD(T) origin peak position for the $a^3B_1$ state is 2.475 eV eBE, indicated by a dashed arrow in Fig. 2b. The calculated VDE of the triplet state is 3.401 eV, which is not accessible with our laser photon energy. The intensity at the VDE is calculated by Franck–Condon factors to be approximately $10^5$ times higher than that at the origin. Based upon this estimate, the intensity of the triplet origin is too weak to be observed with our apparatus, even if there were no other obscuring features. Additionally, the expected triplet origin occurs at electron binding energies corresponding to the greatest interference from the $CHCl_2^-$ contaminant. Furthermore, the high energy end of the $X^1A_1$ state progression overlaps the low energy end of the triplet spectrum. These factors effectively render the triplet origin unobservable.

Consequently, we must use only the shape and intensity of the $a\ ^3B_1$ photoelectron spectrum to obtain an estimate of the binding energy of the triplet origin; this origin then gives our best estimate of the singlet–triplet splitting. We simulate the $a^3B_1$ photoelectron spectrum using a range of origin values centered around the calculated 2.475 eV value. Simulations with origins above 2.7 and below 2.3 eV do not reproduce the experimental features and spectral shape without large changes in the calculated optimized geometries of the $X^2B_1$ and $a^3B_1$ states. Therefore, from the agreement of the simulated spectrum with the experimental results and using the EA determined for the $X^1A_1$ state, we estimate $\Delta E_{ST} = 0.9(2)$ eV for $CCl_2$. This value is consistent with singlet–triplet splittings obtained in recent theoretical studies.[29,33,60]

Further detailed analysis of the triplet state progression provides an experimental challenge. The observed peak widths of the resolved $a^3B_1$ state features indicate that each peak contains contributions from several vibrational transitions. Despite this fact, the separation between the resolved transitions is remarkably uniform at 302(11) $cm^{-1}$, a value that is consistent with the calculated frequency of the bending vibration of 296 $cm^{-1}$ and that is also approximately half the calculated (690 $cm^{-1}$) symmetric stretch frequency. Dyke *et al.* calculate substantial anharmonicity in this mode, quite possibly leading to an apparent near 2 : 1 ratio of these frequencies at the higher vibrational levels that are observed in the triplet progressions.[33] Therefore, we might well expect the resultant vibrational progression to appear as a single progression with contributions from both the bending and symmetric stretching vibrations of $a^3B_1$ $CCl_2$.

Our simulations, as well as those carried out earlier by Dyke *et al.*,[33] clearly show a single progression of peaks containing contributions from both the bending and symmetric stretching vibrations of $a^3B_1$ $CCl_2$. The transitions result from overlapping combination bands of the bending vibrational progression built upon successive quanta of the symmetric stretch vibration. Using our simulated spectrum and corresponding vibronic transitions (sticks in Fig. 2b), we determine the vibrational frequencies for the symmetric stretch (~600 $cm^{-1}$) and bending vibrations (~300 $cm^{-1}$), listed in Table 2.

### $CBr_2$

We report the 364 nm photoelectron spectrum of $CBr_2^-$ obtained through the reaction of $CH_2Br_2$ with $O^-$. As with $CCl_2^-$, both $CBr_2^-$ and $CHBr_2^-$ are formed in the reaction of $CH_2Br_2$ with $O^-$ and are not separable with the Wien filter. Thus, we selectively synthesize $CHBr_2^-$ by reacting $CH_2Br_2$ with $OH^-$ and then subtract the $CHBr_2^-$ contribution to the contaminated spectrum. The photoelectron spectrum at $m/z \approx 172$, taken with horizontal polarization and containing both $CBr_2^-$ and $CHBr_2^-$, is compared to the magic-angle spectrum of pure $CHBr_2^-$ in Fig. 3a. The spectrum of $CHBr_2^-$ is highly structured, indicating that the signal at high eBE in the contaminated spectrum is due to $CHBr_2^-$. This correspondence of well-defined peaks enables subtraction of the contaminant from the spectrum. The $CHBr_2^-$ spectrum is scaled to the contaminated $CBr_2^-$ spectrum, assuming that the difference between the two spectra must remain positive and that all of the intensity in the high eBE peaks is due to $CHBr_2^-$. The clean photoelectron spectrum of $CBr_2^-$, mostly free of contamination from $CHBr_2^-$, is also shown in Fig. 3a. After subtraction, we observe one main progression centered at 2.3 eV that we assign to $X^1A_1$ $CBr_2$. Combined with the improved spectral resolution and increased signal-to-noise in this study, the subtraction of $CHBr_2^-$ yields a $CBr_2^-$ spectrum with substantial improvement over the previous photoelectron spectrum of $CBr_2^-$ (Fig. 3b).[26]

The $X^1A_1$ state of $CBr_2$ displays an extended vibrational progression due to the geometry change between the anion and the singlet neutral, as listed in Table 3. This change in geometry also results in poor Franck–Condon overlap between the ground vibrational levels of $X^2B_1$ $CBr_2^-$ and $X^1A_1$ $CBr_2$, and thus we are unable to observe the singlet origin peak in the photoelectron spectrum.

Franck–Condon simulations are employed to aid in the interpretation of the singlet state spectrum (Fig. 3c). Frequencies and anharmonicities of the singlet state were obtained from a recent single vibronic level (SVL) emission study by Reid and co-workers,[52] while parameters for the anion were calculated using B3LYP/6-311++G** (Table 3).[44] The convolution (black trace) of the individual vibronic transitions

 

(green sticks) reproduces the experimental photoelectron spectrum with EA($X^1A_1$ $CBr_2$) = 1.75(15) eV. The geometry change between the anion and the neutral are determined from these simulations. Using as a reference the geometry of the singlet neutral that was determined by the LIF excitation spectrum[17] combined with *ab initio* calculations,[61] we determine the geometry of $X^2B_1$ $CBr_2^-$ (Table 3): the C–Br bond length is 2.09(2) Å, with a Br–C–Br bond angle of 105(4)°.

Franck–Condon simulations reveal that the progression arising from $X^1A_1$ of $CBr_2$ results from overlapping combination bands of the bend built upon successive quanta of the symmetric stretch vibration. The simulated stick spectrum is in good agreement with the peak positions of the $X^1A_1$ manifold observed by SVL emission.[52] The frequency of the symmetric stretch vibration is approximately three times that of the bend, so the spacing between peaks in the photoelectron spectrum roughly corresponds to the frequency of the bending vibration. Analysis of the spectral peak positions supports a bending frequency of approximately 200 $cm^{-1}$, with an uncertainty on the order of the peak width (100 $cm^{-1}$).

It is unclear whether we have any evidence of the triplet state of $CBr_2$ in the spectrum. Upon subtraction of the $CHBr_2^-$ photoelectron spectrum from the contaminated

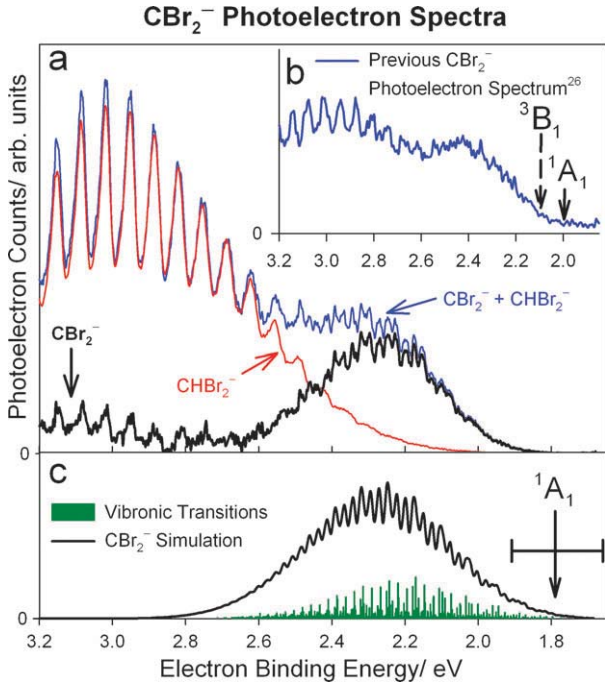


**Fig. 3** $CBr_2^-$ magic-angle photoelectron spectra: A comparison of (a) the new 364 nm spectrum with (b) the previously published 364 nm spectrum.[26] The new photoelectron spectrum is collected at $m/z \approx 172$ and contains contributions from both $CBr_2^-$ and $CHBr_2^-$. The pure $CHBr_2^-$ spectrum is clearly responsible for the progression attributed to the triplet state of $CBr_2$ in the previous spectrum. Subtraction of the $CHBr_2^-$ contribution from the $m/z \approx 172$ spectrum yields the corrected $CBr_2^-$ spectrum. (c) Franck–Condon simulation of the singlet state of $CBr_2$, computed at 350 K. Sticks represent individual vibronic transitions. Solid arrows in (b) and (c) mark the singlet origin in the previous and current studies, respectively, as determined by Franck–Condon analysis. The dashed arrow in (b) marks the incorrect triplet origin assignment of the previous dihalocarbene study.[26]

$CBr_2^-$ spectrum, some residual intensity remains at binding energies greater than 2.6 eV (Fig. 3a). Because the fractional $CHBr_2^-$ contribution in this region is large and because all of the maxima in the subtracted spectrum occur at very nearly the same energy as $CHBr_2^-$ contaminant peaks, we must consider this residual intensity above 2.6 eV eBE to be an artifact of the subtraction. Unfortunately, unlike the $CCl_2^-$ spectrum in which the $CHCl_2^-$ peak appears in the valley between the singlet and triplet states of $CCl_2$, the $CHBr_2^-$ contamination—and thus the residual intensity—occurs in the region in which we expect to see the triplet. Dyke and co-workers predict the $a^3B_1$ origin to be 2.579 eV with a VDE of 3.719 eV (Table 1).[29] Franck–Condon simulations of the $a^3B_1$ $CBr_2$ spectrum using molecular constants calculated by Dyke *et al.*[29] reproduce the peak spacing of the residual features (see ESI†); however, this peak spacing is also the same (within 15 $cm^{-1}$) as that of the contaminant $CHBr_2^-$. Thus, the fact that the contaminant ion completely overlaps the region in which we expect to see the triplet, along with the similarity in $CHBr_2$ and the predicted $a^3B_1$ $CBr_2$ vibrational progressions, conspire to prevent a definitive assignment of the residual peaks. It is clear, however, that the previous $a\ ^3B_1$ origin assignment was incorrect, and the $\Delta E_{ST}$ of $CBr_2$ is greater than previously reported.[26]

## $CI_2$

Finally, we report the 364 nm photoelectron spectrum of $CI_2^-$ obtained through the reaction of $CH_2I_2$ with $O^-$. As with the other halocarbenes, a pure $CHI_2^-$ spectrum is measured, appropriately scaled, and then subtracted from the contaminated spectrum to obtain a clean $CI_2^-$ spectrum. Unlike the other carbenes, we observe a two-photon process with the continuous-wave excitation laser, involving 364 nm photodissociation of $CI_2^-$ to form CI + $I^-$, followed by a second photon detaching an electron from $I^-$. The resulting narrow peak at eBE = 3.06 eV coincides with the known electron affinity of I (EA = 3.059 eV[62]) and confirms the two-photon source of this feature. The presence of the $I^-$ peak indicates that the IC – $I^-$ dissociation energy is substantially less than the photon energy, 3.406 eV. This $I^-$ two-photon feature was not observed in the previous photoelectron spectrum[26] (Fig. 4b), presumably because the laser power in the previous work—a factor of four lower than that used in the present study—was insufficient to make this two-photon process significant. Similar two-photon processes have been observed in anion photoelectron spectroscopy of $O_3^-$, $Ni_3^-$, and $Au_3^-$.[53,63,64] We speculate that 364 nm radiation might produce CX – $X^-$ photodissociation in $CCl_2^-$ and $CBr_2^-$, as well. However, we are unable to observe $Cl^-$ or $Br^-$ photodissociation products because the electron affinity of Cl (EA = 3.613 eV[65]) exceeds the laser photon energy, and 351 nm photodetachment of $Br^-$ (EA(Br) = 3.364 eV[66]) produces electrons with kinetic energy that is too low to be transmitted through the hemispherical electron analyzer.

The photoelectron spectrum is dominated by $CHI_2^-$, which has a broad spectral band spanning approximately 1 eV. As seen in Fig. 4a, there is some residual structure left after the subtraction of $CHI_2^-$ features at binding energies below 3 eV.

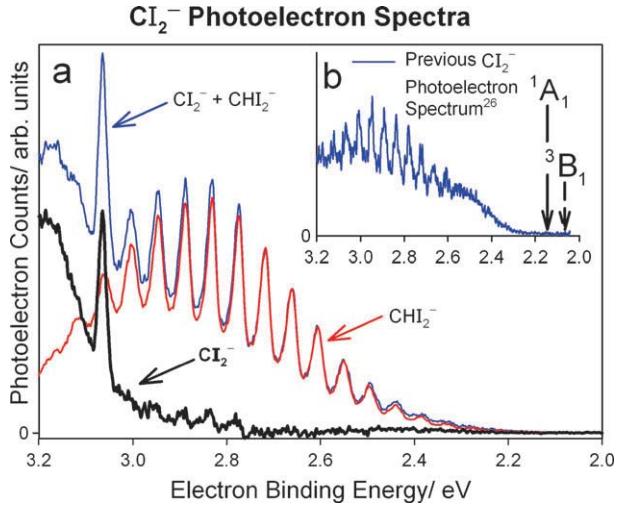


**Fig. 4** $CI_2^-$ 364 nm photoelectron spectra: a comparison of (a) the new magic-angle spectrum and (b) the previously published spectrum.[26] The previous singlet and triplet origin assignments are marked with solid and dashed arrows, respectively, in (b). The photoelectron spectrum collected at $m/z \approx 266$ contains both $CI_2$ and $CHI_2$. The pure $CHI_2^-$ spectrum is clearly responsible for the progression attributed to the triplet state of $CI_2$ in the previous spectrum.[26] Subtraction of the $CHI_2^-$ contribution from the $m/z \approx 266$ spectrum yields the corrected $CI_2^-$ spectrum.

As with $CBr_2^-$, the residual peaks mimic the $CHI_2^-$ spectrum. The remaining broad, structureless feature is attributed to $CI_2^-$, but the lack of resolved features and limited electron energy range preclude any further assignment. Calculations performed by Dyke *et al.* predict the electron affinity of $CI_2$ to be 2.1 eV and the $a^3B_1$ origin to be 2.5 eV with a VDE of 3.5 eV.[29] After the subtraction of the $CHI_2$ progression, we find no significant photoelectron signal below 3.0 eV, and can only claim that $EA(CI_2) < 3$ eV. It is clear that the previous origin assignments[26] for the $CI_2$ singlet and triplet states were actually components of the $CHI_2^-$ photoelectron spectrum, and the assignments were incorrect.

## Conclusion

We have carried out studies of the photoelectron spectra of a series of dihalocarbene anions $CX_2^-$ and the corresponding dihalomethyl anions $CHX_2^-$, where X = Cl, Br, or I. The present results provide a definitive explanation for the incorrect conclusions drawn in the earlier publication from our group: there was undetected dihalomethyl anion contamination in the $CX_2^-$ ion beams.[26] In all three dihalocarbene systems, significant contamination from the related dihalomethyl radical is present and must be subtracted. A contribution from dihalomethyl radicals was present but not identified in previous photoelectron studies, which resulted in the incorrect assignment of the triplet features in all three dihalocarbene systems.

We clearly observe both the $X^1A_1$ and the $a^3B_1$ electronic states of the $CCl_2$ carbene in our current photoelectron spectra. All major peaks in the singlet state are assigned and are consistent with previous experimental spectroscopic parameters for neutral $CCl_2$. The electron affinity of $X^1A_1$ $CCl_2$ is 1.593(6) eV. The triplet state of $CCl_2$ is more complicated, and it is difficult to extract any parameters because of the large changes in geometry between the $X^2B_1$ state of the anion and the $a^3B_1$ state of the neutral. However, simulations of the resolved vibrational spectra at large vibrational quantum numbers yield $a^3B_1$ $CCl_2$ symmetric stretch and bending frequencies of $\sim$600 $cm^{-1}$ and $\sim$300 $cm^{-1}$, respectively. Based on our experimental observations and simulations, we estimate $\Delta E_{ST}$ to be 0.9(2) eV, consistent with recent high-level theoretical calculations. The photoelectron spectra of $CBr_2^-$ and $CI_2^-$ are much more difficult to interpret quantitatively because of the large overlap of the $CHX_2^-$ photoelectron spectrum with that of the singlet and triplet states of the carbene radicals. This contamination, as well as the large geometry differences between the anion and the neutral dihalocarbenes, hinders accurate photoelectron spectroscopic determinations of the $\Delta E_{ST}$ values for these heavier halocarbenes.

The present studies unequivocally resolve the discrepancy between our earlier $CCl_2$ singlet–triplet splitting measurements[26] and numerous subsequent calculations,[29,33,60,67] showing that the previously reported $CCl_2$, $CBr_2$ and $CI_2$ singlet–triplet splittings and $EA(CI_2)$ were in error. A more detailed report of the $CHX_2^-$ halomethyl anion photoelectron spectra will appear in the near future.[36]

## Acknowledgements

We are pleased to acknowledge generous support for this work from the US National Science Foundation and the US Air Force Office of Scientific Research. KME gratefully acknowledges funding from the U.S. Department of Energy, Office of Science, Office of Basic Energy Sciences, Chemical Sciences, Geosciences, and Biosciences Division; a JILA Visiting Fellowship; and sabbatical support from the University of Nevada, Reno.

## References

1 W. Kirmse, *Carbene Chemistry*, Academic Press, New York, 1971.
2 R. A. Moss and M. Jones, in *Carbenes*, ed. R. A. Moss and M. Jones, John Wiley & Sons, New York, 1975.
3 R. A. Moss and M. Jones, in *Reactive Intermediates*, New York, 1978.
4 W. T. Borden, in *Diradicals*, John Wiley & Sons, New York, 1982.
5 L. Andrews, *J. Chem. Phys.*, 1968, **48**, 979.
6 D. J. Clouthier and J. Karolczak, *J. Phys. Chem.*, 1989, **93**, 7542.
7 D. E. Tevault and L. Andrews, *J. Mol. Spectrosc.*, 1975, **54**, 110.
8 V. E. Bondybey and J. H. English, *J. Mol. Spectrosc.*, 1980, **79**, 416.
9 J. I. Choe, S. R. Tanner and M. D. Harmony, *J. Mol. Spectrosc.*, 1989, **138**, 319.
10 M. Fujitake and E. Hirota, *J. Chem. Phys.*, 1989, **91**, 3426.
11 S. L. Xu and M. D. Harmony, *Chem. Phys. Lett.*, 1993, **205**, 502.
12 L. Andrews and T. G. Carver, *J. Chem. Phys.*, 1968, **49**, 896.
13 R. C. Ivey, P. D. Schulze, T. L. Leggett and D. A. Kohl, *J. Chem. Phys.*, 1974, **60**, 3174.
14 V. E. Bondybey, *J. Mol. Spectrosc.*, 1977, **64**, 180.
15 S. K. Zhou, M. S. Zhan, J. L. Shi and C. X. Wang, *Chem. Phys. Lett.*, 1990, **166**, 547.
16 R. Schlachta, G. Lask, A. Stangassinger and V. E. Bondybey, *J. Phys. Chem.*, 1991, **95**, 7132.
17 S. L. Xu and M. D. Harmony, *J. Phys. Chem.*, 1993, **97**, 7465.
18 D. J. Clouthier and J. Karolczak, *J. Chem. Phys.*, 1991, **94**, 1.
19 E. A. Carter and W. A. Goddard, *J. Phys. Chem.*, 1986, **90**, 998.
20 E. A. Carter and W. A. Goddard, *J. Phys. Chem.*, 1987, **91**, 4651.

 

21 E. A. Carter and W. A. Goddard, *J. Chem. Phys.*, 1988, **88**, 1752.
22 G. L. Gutsev and T. Ziegler, *J. Phys. Chem.*, 1991, **95**, 7220.
23 N. Russo, E. Sicilia and M. Toscano, *J. Chem. Phys.*, 1992, **97**, 5031.
24 V. M. Garcia, O. Castell, M. Reguero and R. Caballol, *Mol. Phys.*, 1996, **87**, 1395.
25 A. Gobbi and G. Frenking, *J. Chem. Soc., Chem. Commun.*, 1993, 1162.
26 R. L. Schwartz, G. E. Davico, T. M. Ramond and W. C. Lineberger, *J. Phys. Chem. A*, 1999, **103**, 8213.
27 F. T. Chau, D. K. W. Mok, E. P. F. Lee and J. M. Dyke, *ChemPhysChem*, 2005, **6**, 2037.
28 K. Sendt and G. B. Bacskay, *J. Chem. Phys.*, 2000, **112**, 2227.
29 E. P. F. Lee, J. M. Dyke and T. G. Wright, *Chem. Phys. Lett.*, 2000, **326**, 143.
30 S. A. Drake, J. M. Standard and R. W. Quandt, *J. Phys. Chem. A*, 2002, **106**, 1357.
31 M. L. McKee and J. Michl, *J. Phys. Chem. A*, 2002, **106**, 8495.
32 J. Liang, X. L. Kong, X. Y. Zhang and H. Y. Li, *THEOCHEM*, 2004, **672**, 133.
33 J. M. Dyke, E. P. F. Lee, D. K. W. Mok and F. T. Chau, *ChemPhysChem*, 2005, **6**, 2046.
34 G. Tarczay, T. A. Miller, G. Czako and A. G. Csaszar, *Phys. Chem. Chem. Phys.*, 2005, **7**, 2881.
35 P. Seal and S. Chakrabarti, *Chem. Phys.*, 2007, **332**, 232.
36 K. M. Vogelhuber, S. W. Wren, A. B. McCoy, K. M. Ervin and W. C. Lineberger, to be published.
37 K. M. Ervin and W. C. Lineberger, in *Advances in Gas Phase Ion Chemistry. Volume 1*, ed. N. G. Adams and L. M. Babcock, JAI Prerss, Greenwich, CT, 1992, p. 121.
38 D. G. Leopold, K. K. Murray, A. E. S. Miller and W. C. Lineberger, *J. Chem. Phys.*, 1985, **83**, 4849.
39 K. M. Ervin, J. Ho and W. C. Lineberger, *J. Chem. Phys.*, 1989, **91**, 5974.
40 C. S. Feigerle, PhD Thesis, University of Colorado, 1983.
41 D. M. Neumark, K. R. Lykke, T. Andersen and W. C. Lineberger, *Phys. Rev. A*, 1985, **32**, 1890.
42 C. E. Moore, *Atomic Energy Levels*, Vol. II, NSRDS-NBS Vol. 35, US Govt Printing Office, Washington, D.C., 1971.
43 J. Cooper and R. N. Zare, *J. Chem. Phys.*, 1968, **48**, 942.
44 G. W. T. M. J. Frisch, H. B. Schlegel, G. E. Scuseria, M. A. Robb, J. R. Cheeseman, J. A. Montgomery Jr, T. Vreven, K. N. Kudin, J. C. Burant, J. M. Millam, S. S. Iyengar, J. Tomasi, V. Barone, B. Mennucci, M. Cossi, G. Scalmani, N. Rega, G. A. Petersson, H. Nakatsuji, M. Hada, M. Ehara, K. Toyota, R. Fukuda, J. Hasegawa, M. Ishida, T. Nakajima, Y. Honda, O. Kitao, H. Nakai, M. Klene, X. Li, J. E. Knox, H. P. Hratchian, J. B. Cross, V. Bakken, C. Adamo, J. Jaramillo, R. Gomperts, R. E. Stratmann, O. Yazyev, A. J. Austin, R. Cammi, C. Pomelli, J. W. Ochterski, P. Y. Ayala, K. Morokuma, G. A. Voth, P. Salvador, J. J. Dannenberg, V. G. Zakrzewski, S. Dapprich, A. D. Daniels, M. C. Strain, O. Farkas, D. K. Malick, A. D. Rabuck, K. Raghavachari, J. B. Foresman, J. V. Ortiz, Q. Cui, A. G. Baboul, S. Clifford, J. Cioslowski, B. B. Stefanov, G. Liu, A. Liashenko, P. Piskorz, I. Komaromi, R. L. Martin, D. J. Fox, T. Keith, M. A. Al-Laham, C. Y. Peng, A. Nanayakkara, M. Challacombe, P. M. W. Gill, B. Johnson, W. Chen, M. W. Wong, C. Gonzalez and J. A. Pople, *Gaussian 03*, Revision B01, Gaussian Inc., Wallingford, CT, 2004.
45 J. A. Pople, M. Headgordon and K. Raghavachari, *J. Chem. Phys.*, 1987, **87**, 5968.
46 T. H. Dunning, *J. Chem. Phys.*, 1989, **90**, 1007.
47 D. E. Woon and T. H. Dunning, *J. Chem. Phys.*, 1993, **98**, 1358.
48 A. D. Becke, *J. Chem. Phys.*, 1993, **98**, 5648.
49 C. T. Lee, W. T. Yang and R. G. Parr, *Phys. Rev. B: Condens. Matter Mater. Phys.*, 1988, **37**, 785.
50 K. M. Ervin, *PESCAL Fortran program*, 2008.
51 M. L. Liu, C. L. Lee, A. Bezant, G. Tarczay, R. J. Clark, T. A. Miller and B. C. Chang, *Phys. Chem. Chem. Phys.*, 2003, **5**, 1352.
52 C. Tao, C. Mukarakate and S. A. Reid, *J. Mol. Spectrosc.*, 2007, **241**, 136.
53 J. Ho, K. M. Ervin and W. C. Lineberger, *J. Chem. Phys.*, 1990, **93**, 6987.
54 P. Chen, in *Unimolecular and Bimolecular Reaction Dynamics*, ed. C.-Y. Ng, T. Baer and I. Powis, John Wiley & Sons, Chichester, 1994, p. 371.
55 K. M. Ervin, T. M. Ramond, G. E. Davico, R. L. Schwartz, S. M. Casey and W. C. Lineberger, *J. Phys. Chem. A*, 2001, **105**, 10822.
56 J. Lee and J. J. Grabowski, *Chem. Rev.*, 1992, **92**, 1611.
57 K. K. Murray, D. G. Leopold, T. M. Miller and W. C. Lineberger, *J. Chem. Phys.*, 1988, **89**, 5442.
58 C. Mukarakate, Y. Mishchenko, D. Brusse, C. Tao and S. A. Reid, *Phys. Chem. Chem. Phys.*, 2006, **8**, 4320.
59 J. C. Bopp, J. R. Roscioli, M. A. Johnson, T. M. Miller, A. A. Viggiano, S. M. Villano, S. W. Wren and W. C. Lineberger, *J. Phys. Chem. A*, 2007, **111**, 1214.
60 C. J. Barden and H. F. Schaefer, *J. Chem. Phys.*, 2000, **112**, 6515.
61 C. W. Bauschlicher, *J. Am. Chem. Soc.*, 1980, **102**, 5492.
62 D. Hanstorp and M. Gustafsson, *J. Phys. B*, 1992, **25**, 1773.
63 S. E. Novick, P. C. Engelking, P. L. Jones, J. H. Futrell and W. C. Lineberger, *J. Chem. Phys.*, 1979, **70**, 2652.
64 K. M. Ervin, J. Ho and W. C. Lineberger, *J. Chem. Phys.*, 1988, **89**, 4514.
65 J. D. D. Martin and J. W. Hepburn, *J. Chem. Phys.*, 1998, **109**, 8139.
66 C. Blondel, P. Cacciani, C. Delsart and R. Trainham, *Phys. Rev. A*, 1989, **40**, 3698.
67 B. Hajgato, H. M. T. Nguyen, T. Veszpremi and M. T. Nguyen, *Phys. Chem. Chem. Phys.*, 2000, **2**, 5041.